Fátima Alexandra Morais Zorro

Bachelor in Micro and Nanotechnologies Engineering

Spatial atomic layer deposition of LiPON thin films

Dissertation submitted in partial fulfillment
of the requirements for the degree of

Master of Science in
Micro and Nanotechnologies Engineering

Adviser: Dr. Lucas Haverkate, Research Scientist,
Holst Centre, Netherlands
Co-adviser: Dr. Joana Maria Dória Vaz Pinto, Assistant Professor,
Faculdade de Ciências e Tecnologia da Universidade
Nova de Lisboa, Portugal

Examination Committee

Chairperson: Dr. Rodrigo Ferrão de Paiva Martins
Raporteurs: Dr. Rui Alberto Garção Barreira do Nascimento Igreja
Dr. Lucas Haverkate

FACULDADE DE
CIÊNCIAS E TECNOLOGIA
UNIVERSIDADE NOVA DE LISBOA

September, 2018

Spatial atomic layer deposition of LiPON thin films

This document was created using the (pdf)LaTeX processor, based in the "novathesis" template[1], developed at the Dep. Informática of FCT-NOVA [2].
[1] `https://github.com/joaomlourenco/novathesis` [2] `http://www.di.fct.unl.pt`

We won’t have a society if
we destroy the environment.

Margaret Mead

Acknowledgements

In this section I would like to thank everyone that somehow made a difference through these last five years of my life and helped me to be who I am today. A big thank you to you all.

Firstly, I would like to thank to my coordinator, Dr. Lucas Haverkate for accepting me in this project, his guidance and support which helped me to overcome the challenges that were involved in this work.

A special thanks to Dr. Sandeep Unnikrishnan for his patience, understanding and knowledge shared during meetings.

To Dr. Mahmoud Ameen for his availability to guide me through the last months, bringing new ideas and of course good mood.

To Prof. Fred Roozeboom, for all his critical sense, suggestions and informations provided though the thesis that contributed to all the project improvement.

To Mr. Frank Grob for the hours spent in the POP-2 reactor preparing the system, finding and solving problems, teaching me in general how the reactor works in terms of software and hardware.

To Dr. Michal Tulodziecki for teaching me how to work in a glove box, assemble coin cells and assistance through some initial electrochemical analysis.

Of course, I am very thankful to Dr. Joana Vaz Pinto, which besides teaching me a significant part of what I know about micro and nanotechnologies, also accepted the challenge of being my thesis supervisor, was always interested and providing help through all the difficulties.

To my Holst Centre colleagues that were by my side during this challenge, specially to my battery team colleagues Karan Narayan for our walks in HTC and to Andrea Bracesco for his good mood and cheering ability.

Ao Dr. Paulo Ferreira do INL que me aguçou a curiosidade sobre baterias, ao Dr. Sebastian Calderon pelo conhecimento transmitido e à Cinthya Blois, a minha brasileira preferida pelas conversas e conselhos.

Não posso deixar de agradecer ao Prof. Rodrigo Martins e à Prof. Elvira Martins por tomarem a iniciativa de criar este curso, sem o qual eu não estaria aqui, por me darem o privilégio de serem meus professores e pela visibilidade que transmitem ao mesmo.

Quero dar um enorme obrigado à minha família que para além de me terem possibilitado a oportunidade de ir para a faculdade, sempre apoiaram as minhas ideias loucas e ficaram com o coração nas mãos, por me aturarem, animarem, distraírem e no fundo por serem a família que são para mim.

A todos o meus colegas da "Casa da francesinha" que viveram comigo, pelas festas e jantares em especial ao Sérgio Gomes e à Ana Ortiz Pérez, pelo seu enorme coração, conversas e boa disposição. Also to my FCT friends, specially to Catarina Costa, Diogo Coelho, Tiago Gonçalves, Jaissica Vassantrai, Leonor Matias and João Pereira for the lunches together, cinema, work groups, the availability to talk and help me, despite of the fact that we are not always together, when we meet again looks like we never stopped talking.

Ao departamento de ciências dos materiais por criarem e tomarem parte em eventos, como a "Ciência Viva" e "Expo FCT" nos quais eu tive a oportunidade de participar e estender as minhas relações com outros colegas.

To my Erasmus friends, for the different cultures that you brought to me, specially to Tomoki Seki, the nicest and chillest Japanese person that I have ever met, for the Disneyland journey, going to Portugal to meet me, and remembering to talk once in a while.

To José Virtuoso since he was always on my side through this 5 years and no one understood better my dramas than him. For the good and bad moments, lunches, dinners, adventures, holidays, intensive study days, and so much more events that is impossible to describe it all here.

Abstract

In the last few years, with the advance of electrical vehicles and number of devices needing safe batteries especially in the medical field, a more efficient way to store energy is necessary.

Despite the fact that conventional lithium batteries present high conductivity values, they do not exhibit enough charging/discharging speed and also include dangerous components to health. To overcome those challenges, thin film solid-state batteries are considered a promising candidate. However, this all-solid-state battery concept exhibits too low energy density, pushing the technology towards 3D structures and developing 3D all-solid-state lithium-ion batteries (ASSBs).

This thesis describes the development of a pinhole-free solid-state lithium-ion electrolyte through *spatial*, to pave the way for cost effective and scalable 3D ASSBs.

The produced films are thoroughly characterized to find the relation between deposition parameters and film quality in terms of thickness, reproducibility, uniformity, composition and conductivity. The obtained LiPON, being deposited with the fast *spatial* ALD process, offers ionic conductivity of 1.55 (± 0.14) x 10^{-7} S/cm and electronic conductivity of 1.86 x 10^{-13} S/cm, being a promising solid electrolyte layer for next generation lithium-ion batteries.

Keywords: Solid state battery, Thin film technology, Lithium, *spatial* atomic layer deposition, Electrolyte.

Resumo

Nos últimos anos, com o avanço das tecnologias relacionadas com veículos elétricos e aumento do número de dispositivos que necessitam de baterias seguras, especialmente no âmbito da medicina, métodos mais eficientes de armazenar energia são necessários.

Apesar das baterias de lítio apresentarem elevados valores de condutividade, não são suficientemente rápidas em termos de carga/descarga e incluem componentes perigosos à saúde. Para ultrapassar estes desafios, as baterias de filme fino constituem um candidato bastante promissor. No entanto, o conceito de bateria de filme fino exibe reduzidas densidades de energia, conduzindo à evolução da tecnologia para as estruturas 3D e desenvolvendo as baterias 3D de iões de lítio em estado sólido.

Esta tese descreve o desenvolvimento de um eletrólito de lítio de estado sólido através da técnica de *spatial* Atomic Layer Deposition (ALD), de forma a posteriormente ser possível desenvolver baterias 3D de estado sólido economicamente viàveis, e escaláveis.

Os filmes produzidos foram metódicamente analisados de modo a relacionar os parametros de deposição com a qualidade dos mesmos em termos de espessura, reproducibilidade, uniformidade, composição e condutividade. Os filmes de LiPON obtidos, sendo depositados por *s* ALD, oferecem condutividades iónicas de 1.55 (± 0.14) x 10^{-7} S/cm e condutividades eletrónicas de 1.86 x 10^{-13} S/cm, constituindo assim eletrólitos sólidos para a próxima geração de baterias de iões de lítio.

Palavras-chave: Baterias de estado sólido, Tecnologia de filmes finos, Lítio, *s*ALD, Eletrólito.

Contents

List of Figures

List of Tables

Acronyms

3D	3 dimensional
ALD	Atomic layer deposition
ASSBs	All-solid-state batteries
CPE	Constant phase element
CVD	Chemical vapour deposition
EDX	Energy dispersive x-ray spectroscopy
EIS	Electrochemical impedance spectroscopy
GPC	Growth per cycle
LIB	Lithium-ion battery
LiOxy	Lithium and Oxygen source
LiPON	Lithium phosphorus oxynitride
MEM	Metal-electrolyte-metal
NitPhO	Nitrogen, Phosphorus and Oxygen source
RF	Radio frequency
RPM	Rotations per minute
sALD	spatial atomic layer deposition
SEI	Solid electrolyte interface
SEM	Scanning electron microscope
XPS	X-ray photoelectron spectroscopy

Objective

3D solid-state lithium-ion batteries exhibit a promising energy density and charging speed among other properties when compared with conventional batteries being the best option for applications in a wide range of stored energy requirements suchs as wireless autonomous devices (mWh), in the medical field (Wh) and in electric vehicles (kWh), hence are crucial for daily life. The aim of this thesis is the development of a solid-state electrolyte in the lithium phosphorus oxynitride family by thermal spatial atomic layer deposition, more precisely:

- Investigate the influence of film deposition process parameters on material properties.
- Characterization of the electrolyte performance.
- Incorporate electrolyte in a battery cell plus characterization.

In an industrial point of view, some of the goals are to reach an ionic conductivity superior to 10^{-7} S/cm and an electronic conductivity inferior to 10^{-13} S/cm.

Work structure

To simplify the understanding of this thesis it is divided as follows: the motivation which explains the importance of the energy in people daily basis and in special, on 3D all-solid-state batteries. The introduction where it is enlightened the basics of batteries, electrolytes and *spatial* atomic layer deposition, characterization methods and the state of the art in the current technology. Methodology describes, in general, the procedures followed to produce the samples and characterize them. Finally, the results are presented where the electrolyte is characterized in terms of process parameters impact in the thin film growth, uniformity, substrate effect, roughness, composition, conductivity, and crystal structure.

To finish conclusions and future perspectives are presented.

Motivation

The term battery was invented in 1749 by Ben Franklin and the concept was made practical in 1800 by Alessandro Volta which created the first voltaic cell. Since then many scientists as John Daniell, Gaston Planté, between many others, search for different ways to increase the performance, capacity and lifetime of these devices conjugating different materials and ways to assemble them, contributing for the development of this technology. More recently, in 1989, John B. Goodenough developed the lithium ion battery, which significantly decreased the production costs and increased their energy densities making it a greener source of energy available for everyone. Nowadays these devices are part of the modern world and can be found in most of portable applications not just around houses but also in autonomous wireless devices, in the medical environment: pacemakers, defibrillators, in fire fighting and emergency response, military use, construction, logistics and transports.

Can you imagine a single day in your life without batteries?

1 Introduction

1.1 Batteries

The development of society and technology instilled an increase in energy demand in the renewable and non-renewable sources as shown in figure 1.1. In the field of non-renewables the exploration and exploitation of oil, coal and natural gas leads to serious environmental problems including global warming and air pollution. Worldwide efforts are being developed to further obtain a sustainable energy supply. Thus research on renewable sources has become essential, as is the exploration of ways to store it. Among the various forms to save energy, one of the most attractive devices that assure storage are batteries, in particular rechargeable batteries [1, 2].

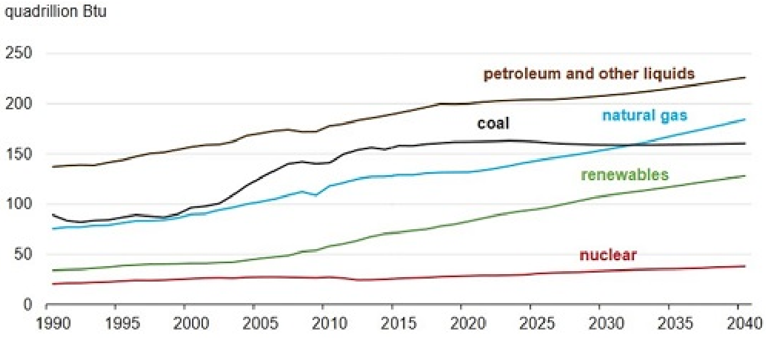

Figure 1.1: Total world energy consumption projection by energy source [3].

Batteries are defined as electrochemical storage devices, that can store energy when there is an excess and release energy when it is necessary, converting chemical into electrical energy, and vice-versa.

To assure proper operation of batteries, the electrolyte must be a good ionic conductor and an electrical insulator since the discharge cycle is described by the diffusion of ions through the electrolyte, from the anode to the cathode while electrons flow in an outer circuit powering the device connected to the battery. In a charge cycle, the same mechanisms occur but in opposite directions, electrons, and ions flow from the cathode to the anode [4].

Depending upon usability, batteries are available in two variants: primary which can only be used once due to the irreversible changes in the electrolyte or secondary also known as rechargeable, which can go through multiple charging and discharging cycles during his lifetime.

Between many types of materials used to form these devices, one of the most accepted is lithium due to its properties as high energy density, good performance and memory effect absence when included in a battery system [5].

1.1.1 Lithium Ion Batteries

Lithium-ion batteries (LIBs) were created by John Goodenough in 1970 and first commercialized by Sony Corporation in 1990. When compared with traditional devices such as nickel-cadmium or lead acid battery, LIBs store triple of the energy, have lower charging times, longer lifetimes, higher energy densities, autonomy, and better ability to be miniaturized [2].

Typically, these electrochemical devices are composed by an anode (negative electrode) a cathode (positive electrode) an electrolyte and two current collectors. Lithium batteries can be divided in two categories according the electrolyte's physical state: if liquids are considered as wet lithium ion batteries and in the solid case as all-solid-state batteries (ASSB).

Lithium-ion batteries have undergone major developments over the years regarding their electrolytes: wet LIBs despite the great ionic conductivity, embody major hazards for health since organic liquid electrolytes are flammable, which might lead to explosions. It is as well challenging to use them with high-energy density electrodes, particularly lithium metal due to dendrite formation. This way they are neither easy to miniaturize nor to produce for flexible devices. In order to safely integrate LIBs into medical applications and electric vehicles, the ASSBs were developed. Solid-state electrolytes enable high-energy density electrodes such as lithium metal, leading to increased energy densities. However, planar thin film solid state batteries require stacking of multiple layers, which are not easy to manufacture with high yield and low cost [1, 6].

The research is now focused on the development of three-dimensional solid-state lithium-ion batteries, besides the advantages of the solid state, also exhibit a higher energy density. The three categories of batteries mentioned above will be addressed with further detail in the following sub-chapters.

1.1.1.1 Wet Lithium Ion Batteries

Wet LIBs are composed of a non-aqueous Li electrolyte embedded in a separator positioned between the anode and the cathode. The liquid electrolyte confers high ionic conductivities while the separator is used to avoid the short-circuit between the electrodes.

Liquid electrolytes confer significant advantages to their ionic conductivity. In contrast, there are major concerns associated with the safety of these batteries. Occasionally, the liquid reacts with the electrodes, establishing a solid electrolyte interface (SEI) layer. Besides, during abusive use like overcharging, lithium metal may be formed onto the anode, which leads to dendrite formation that penetrate through the separator and lead to short circuiting of the electrodes and possibly explosion of the device where the battery is inserted [7, 8].

1.1.1.2 Thin Film All Solid State Batteries

Regarding their structures, solid and liquid batteries are vastly identical as shown in figure 1.2. In the solid device, a separator is not required since the electrodes are separated by the solid electrolyte. The main physical difference is their size and thickness: in liquid electrolyte batteries their area cannot be smaller than the coin cell dimensions, and the separator can reach 20 µm thickness, while thin film ASSBs can reach a few milimeters of total area and the electrolyte has a maximum of typically 1 µm thickness [9].

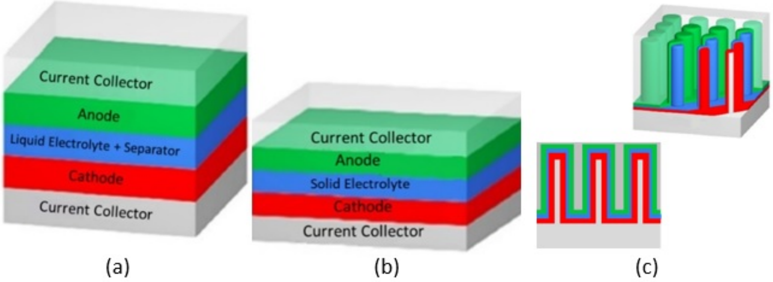

Figure 1.2: (a) Constitution of wet lithium ion batteries.(b) Different layers in all-solid-state batteries. (c) Structure of a 3D ASSB configured in a pore array and in a pillar array [9].

These characteristics affect their properties: ASSB are safer, have a much longer cycle life, can be applied in microelectronic devices, have high temperature stability but lower ionic conductivity. This is not very significant considering that these devices are much thinner, creating short diffusion lengths, and low energy density which can be improved by using 3 dimensional (3D) all-solid-state batteries [10].

1.1.1.3 3D All Solid State Batteries

Within a battery electrode, a 3D nanoarchitecture can give enhanced porosity, increasing the active surface area by 10 to 30 times without changing the macroscopic dimension. It can be created in a conventional planar substrate, which means that with similar internal current densities, a much higher total battery current can be obtained [11]. The challenge is to develop deposition techniques that give conformal, uniform, easy-to-produce thin films, with high throughput and compatible with battery material [12].

1.1.2 Atomic Layer Deposition

Multiple techniques have been developed to deposit thin-film solid-state electrolytes, including radio frequency (RF) magnetron sputtering, chemical vapor deposition (CVD), pulsed layer deposition, and atomic layer deposition (ALD). This last technique is a particular case of CVD.

1.1.2.1 Conventional ALD

In conventional ALD, precursors are injected time-sequentially in the deposition zone, reacting one at a time with the active sites on the substrate surface through selective and self-limiting half-reactions. Each half-cycle is separated by purge steps to remove all remaining precursor and reaction products in the gas phase formed in the previous half-cycle [13]. The nature of ALD precursors allows high-quality material deposition at lower temperatures than with CVD, even near room temperature [14].

Conventional ALD can be defined by its particular temperature dependence. The growth takes place only in a characteristic temperature window since, at too low temperatures, precursor molecules cannot be sufficiently activated, or desorption can be too slow. At high temperatures, precursors can decompose at the surface or even before reaching it, and desorption can be too fast during the purge step. The entire process mostly takes place under vacuum, at high temperatures (thermal ALD), and optimally with a plasma source coupled (plasma enhanced ALD) to improve the deposition [15].

This technique presents a relevant disadvantage which consists in the reactor purging time, a consuming step that severely limits the deposition speed of conventional ALD. This drawback has been overcome by spatial atomic layer deposition (sALD).

1.1.3 *Spatial* ALD

In *s*ALD the dosage of precursors occurs in different space-divided zones of the reactor and a moving substrate is sequentially exposed to each of these zones (see figure 1.3). Spatially dividing them by a nitrogen gas curtain, the purge step is no longer necessary and deposition rates can be up to two orders of magnitude faster (from 0.01 nm/s to 1.0 nm/s) [16].

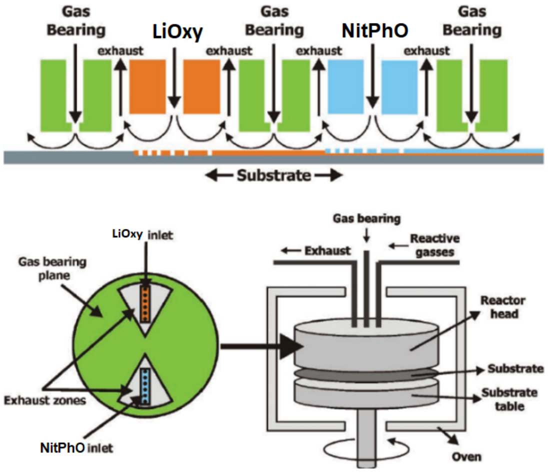

Figure 1.3: Schematic drawing of the *s*ALD reactor concept [13].

Additionally, *s*ALD presents the advantage of being easily performed at ambient atmosphere, allowing it to be easier and cheaper to scale up than conventional ALD. This opens the door to widespread industrial applications in high quality films fully suited for device integration in fields within solar energy, energy storage, or smart windows[17].

Though it was not until 2008 that the first scientific article on *s*ALD was published, it has proven to be a very versatile one from the engineering point of view, since many reactors have been reported to date.

1.1.4 Lithium Phosphorus Oxynitride Electrolyte

Solid-state lithium electrolytes have been extensively studied to develop an ASSB. To be an ideal material it must have good ionic conductivity, $\geq 10^{-6}$, negligible electronic conductivity, $\leq 10^{-13}$ and for high voltage cathodes, such as $LiMn_2O_4$ and $LiCoO_2$, have a stability window around 5 V [18].

Lithium phosphorus oxynitride (LiPON) is one of the most suited electrolytes since it presents all the characteristics announced above, also is widely studied and industrially used in lithium battery technology as a solid-state layer.

The LiPON family comprises a wide range of compositions which is inherent in a quaternary phase diagram between Li_2O, Li_3N, P_3N_5 and P_2O_5. Generally, the N-content in the film has a relevant importance in their properties correlating a higher concentration with a higher ionic conductivity and a lower activation energy. In literature, LiPON is usually prepared by reactive radio-frequency magnetron sputter deposition, using lithium phosphate as a target and nitrogen as a reactive gas. There have been some efforts in the past years to increase the ionic conductivity of such layers by using different sputter targets (e.g. mixtures of Li_2O and Li_3PO_4 or by optimizing the deposition parameters (e.g. varying the partial pressure of nitrogen) [18].

Thin films of LiPON were first characterized and investigated for thin-film batteries by Bates et al. who reported a maximum ionic conductivity of 3.3 x 10^{-6} S/cm using radio-frequency sputter deposition to prepare thin-film samples [19].

Any deposition technique based on plasma processes, usually nitrogen plasma in order to incorporate the atoms in the film, cannot be applied in a 3D ASSB as radicals lifetime is very limited: while diffusing down into the pores of the substrate, the radicals recombine. This prevents them from reaching the bottom of the substrate. Thus, it is necessary to investigate deposition methods as atomic layer deposition, using precursors that contain already the the nitrogen atom to form the lithium phosphorus oxynitride films.

The LiPON family materials consists of multiple compounds including Li_2PO_2N and Li_3PO_4. Table 1.1 summarizes the different state-of-the-art electrolytes that belong to the LiPON family and respective ionic conductivities, deposition techniques, and precursors used.

Table 1.1: Different LiPON family electrolytes and respective ionic conductivities, deposition techniques and precursors used.

Electrolyte	Ionic Conductivity (S/cm)	Precursors	Deposition Technique
Li_2PO_2N[19]	1.4×10^{-7}	LiO^tBu+DEPA	Thermal ALD (250 °C)
Li_2PO_2N[19]	1.6×10^{-7}	LiO^tBu+DEPA	Thermal ALD (300 °C)
LiPON [20]	9.3×10^{-8}	LiHMDS+DEPA	Thermal ALD (290 °C)
LiPON [20]	6.6×10^{-7}	LiHMDS+DEPA	Thermal ALD (330 °C)
LiPON [21]	1.7×10^{-6}	Li_3PO_4 (target)	RF Sputtering
Li_3PO_4[22]	1.0×10^{-10}	LiO^tBu+TMP+H_2O	Plasma ALD

In this report we used two precursors, which due to confidentiality issues will be named precursor NitPhO, the source of nitrogen, phosphorus and oxygen, and precursor LiOxy as the lithium and oxygen donor since this combination has yielded LiPON family films previously in literature [19, 20].

2 Materials and Methods

2.1 *s*ALD Setup

The *s*ALD setup is composed of an oven that contains the reactor and is coupled to a glove box as shown in figure 2.1, an exhaust and scrubber system, plasma controls and gas cabinets for the supply of the precursors which are transported through heated pipes to the reactor. The oven has two doors: one opens to the laboratory side and the other to the glove box which allows the depositions to be performed fully in argon atmosphere. The oven is heated by internal circulation of the air or Argon over an electrical heating element. A motor drives the rotation of the wafer table during depositions. All gas pipelines between the oven and valves are wrapped around with an insulating material to prevent heat loss. The glove box is kept with an Argon environment above 3 mbar with O_2 and H_2O levels below 0.5 ppm and is attached to a cooling system to prevent the its overheating. Inside the glove box is a mechanic arm to transfer the substrate and holder into the oven. The reactor itself is composed by a top part (ALD head) and a bottom part (rotating table and substrate holder).

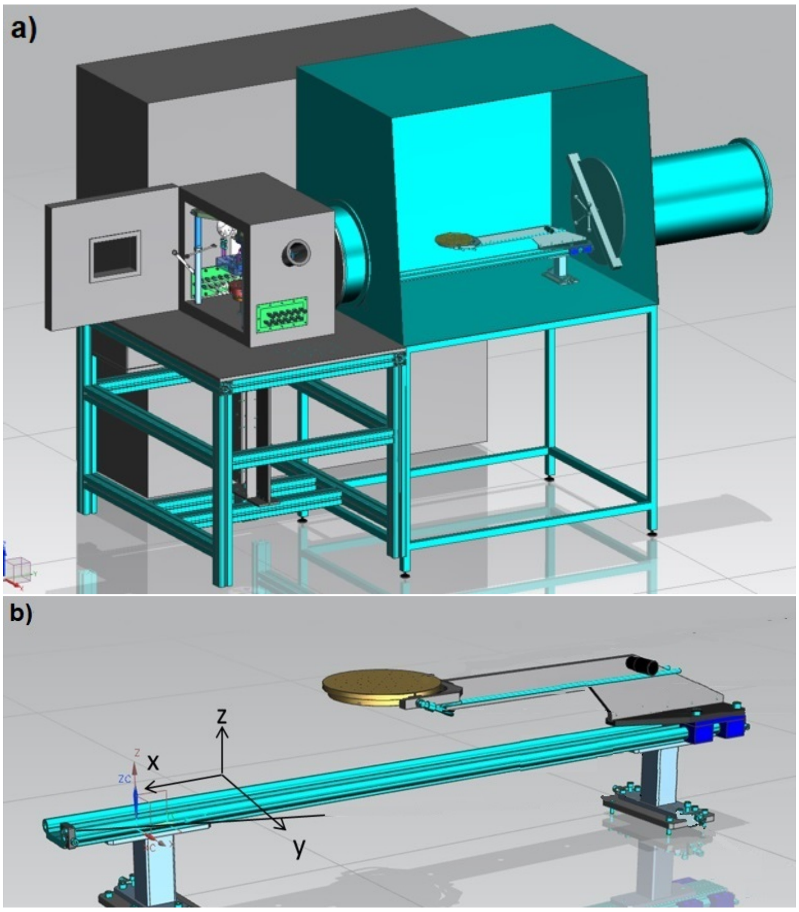

Figure 2.1: (a) 3D scheme of te oven and glovebox.(b) Glove box mechanic arm.

2.2 Substrates

Different substrates have been used in the LiPON depositions. Silicon wafers (<100> orientation, n-type, with 0.005 Ω.cm of resistivity) were used to verify if the combination of precursors would create a solid layer. TiN/Pt or TiN covered Si wafers were then used to characterize the LIPON films, see figure 2.2. The TiN on the first wafers acts as an adhesive conductor and Li-ion diffusion barrier layer between the Pt and Si.

(a) (b)

Figure 2.2: Scheme of the layers: (a)Pt/TiN/Si substrate; (b)TiN/Si substrate.

The Pt and TiN were chosen because they both behave as a current collector with no lithium outdiffusion due to the blocking properties of the TiN layer.

2.3 LIPON depositions

To deposit LiPON, the oven must be uniformly heated until a desired temperature. To load the wafer, the substrate holder must be aligned with the slider arm so it can be taken from the oven into the glove box. Here, the wafer can be placed on the hot substrate holder an be transferred back to the oven onto the rotation table which will push it against the ALD head. All these steps can be found schematically in figure 2.3. During depositions the distance between the sample and the top of the oven is 50 μm.

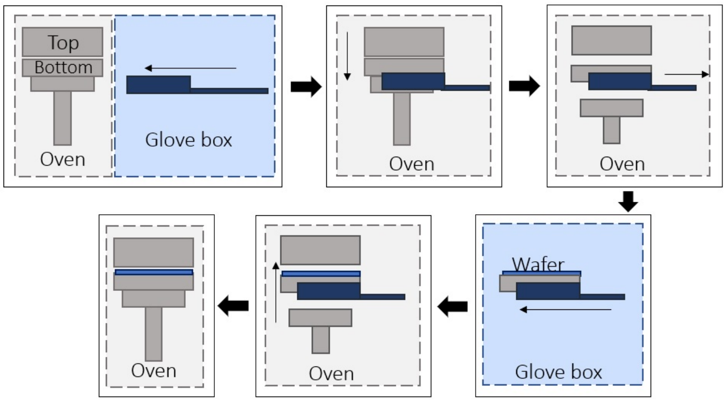

Figure 2.3: Scheme of sample introduction in the oven.

There is a manual verification of the spinning system, making the wafer slightly spin, to avoid bad contact between it and the reactor upper part. If resistance is felt, the wafer must be replaced.

The following settings must be introduced in the computer:
- NitPhO bubbler temperature;
- LiOxy bubbler temperature;
- NitPhO flow ;
- LiOxy flow;
- Rotation speed.

After deposition the substrate holder is again aligned with the robotic arm and the wafer is placed inside the glove box. The procedure is similar to the wafer introduction into the reactor.

2.4 Glove box

After deposition the sample is transferred to another glove box. To transport the sample between glove boxes or for measurement equipment, we used a sealed cubic stainless steel transport box. This protection is needed because the oven is not oxygen free and once opened to remove the sample it releases around 8 ppm of oxygen. The other glove box is more equipped to posteriorly treat the samples for analysis. This equipment is part of a set composed by two glove boxes, one big antechamber, two small antechambers one of them with the possibility of being heated until 80 °C. The glove boxes are in argon environment.

2.5 Scanning Electron Microscopy and Energy Dispersive X-Ray Spectroscopy

2.5.1 Preparation of Samples

To prepare the samples for scanning electron microscopy (SEM) and energy dispersive x-ray spectroscopy (EDX) it is necessary to cut, with a diamond tip pen, a piece of a quarter wafer as represented in figure 2.4.

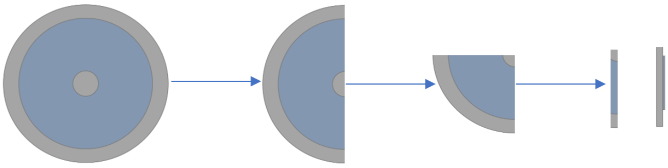

Figure 2.4: Scheme of how the samples are cutted to SEM and EDX analysis.

The small piece is fixed in the sample holder by using carbon tape. Depending on the objective of the characterization the sample can be placed in different ways:
- To analyse the sample's morphology and roughness through SEM or composition through EDX, it is placed on top of the holder with the LiPON layer turning to the top.
- To investigate the sample's cross-section and conformity, it must be placed on

the side of the holder with the LiPON layer facing the outside.

2.5.2 Transfer to equipment

Once the samples are ready, the holder is placed inside the transport box, which is posteriorly closed, taken out and moved near the microscope.

To insert the samples inside the microscope chamber, it is necessary to open the transport box. Air exposure of the samples for around two minutes is unavoidable since the equipment has no glove box attached. This step and the remnant analysis are performed by a designated professional. After characterization, the holder is again placed inside the transport box and samples are disposed.

2.6 X-Ray Photoelectron Spectroscopy

The sample cutting procedure for XPS analysis is identical for SEM and EDX, however, the samples are not placed on a holder. Instead, they are stored in a wafer box which is placed in the transport box and taken to the XPS equipment glove box attached.

The analysis of one sample consists of two surface XPS scans and a depth profile scan. XPs is again performed by designated professionals and posteriorly the samples are discarded. The purpose of XPS in this thesis work is to analyse the elemental composition and bond's atomic coordination of the LiPON thin films.

2.7 Electrochemical Impedance Spectroscopy

2.7.1 Preparation of Samples

For these measurements, a metal-electrolyte-metal (MEM) stack is produced. Sample preparation is again described in section 2.5.1. By using an electron beam evaporator, a 400 nm thick copper film is deposited through a shadow mask with multiple 4 mm diameter openings to form circular top electrodes, defining the device area. PEIS measurements were taken between 1 MHz and 0.1 Hz with an excitation amplitude of 50 mV.

2.7.2 Equipment Setup

The potentiostatic EIS setup is constituted by two probes, placed inside a glove box, a temperature probe, a peltier element, and a power source (see figure 2.5).

To prevent short circuits the tip of one probe is welded with a Sn droplet and after checked that it does not lead to a significant increase in the system total resistance, measurements are performed as illustrated in figure 2.6.

Figure 2.5: Scheme of the EIS setup.

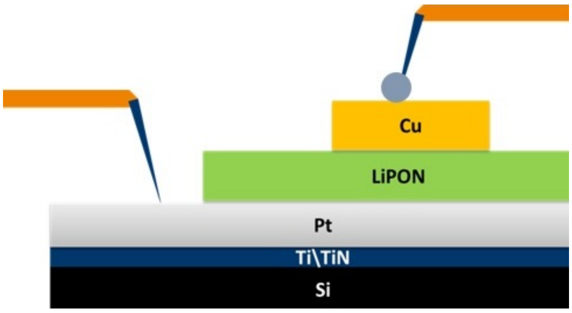

Figure 2.6: Placement of probes in the setup.

3 Results and Discussion

3.1 Process parameters

In total 34 depositions have been performed. We explored the impact of the deposition temperature, speed and precursors flow in chemistry and growth characteristics of NitPhO-LiOxy reaction to obtain a LiPON family member. Before any measurements, SEM was used to determine the average layer thickness and growth rate of deposited thin films, and a general profile, profilometry is used to understand some profiles with further detail. Posteriorly, XPS was used to determine their detailed chemistry, XRD for crystal structure analysis and a double probe station for electrochemical measurements.

3.1.1 Impact of the deposition temperature

Overall is possible to assert that the reaction goes through a non-ideal *s*ALD process, despite self limiting growth as a function of NitPhO and LiOxy precursor parameters, it lacks an obvious temperature window for a constant growth rate.

Figure 3.1 shows that the growth rate decreases across the deposition temperature range from 2.21 Å at T_1 until 0.61 Å at T_4, keeping the remaining settings constant, NitPhO and LiOxy flows at f_3 and f_4, respectively. The process with the mentioned precursors does not exhibit a constant growth window characteristic of a thermally activated reaction and typical in ALD. The calculated growth per cycle (GPC) is lower than what have been reported in literature for ALD-grown LiPON films [20][23] . At lower temperatures the layer thickness is significantly high which suggests the possibility of uncontrolled surface reactions.

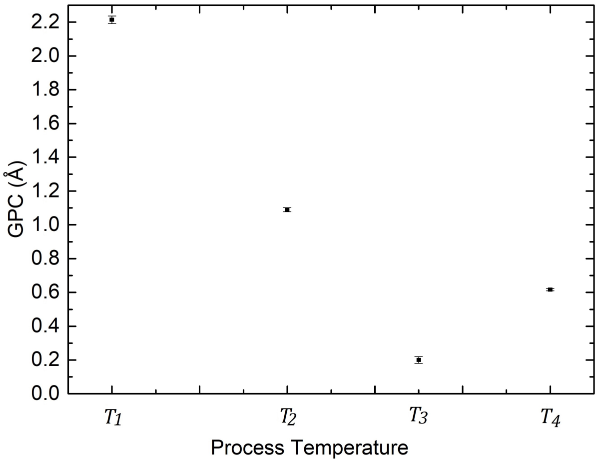

Figure 3.1: Influence of the temperature on the GPC of the films.

3.1.2 Impact of NitPhO flow rate

Figure 3.2 outlines the growth rates measured over 1500 cycles for different NitPhO flows rates while keeping the LiOxy dosage constant and the temperature T_3. It appears that the reaction exhibits a self-limiting behaviour, typical of a *s*ALD process.

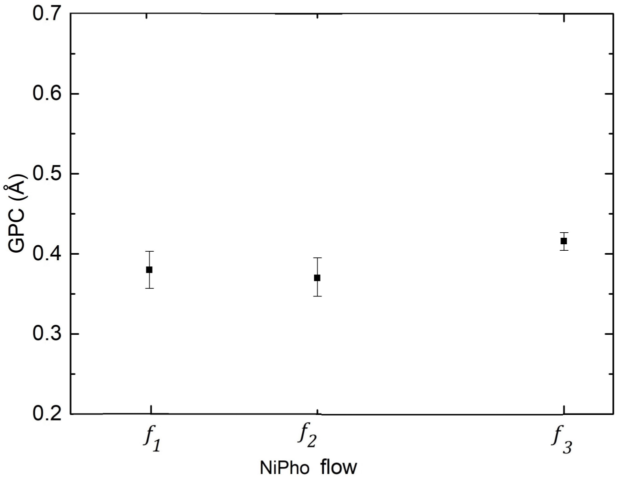

Figure 3.2: GPC according with the NitPhO flow.

3.1.3 Impact of LiOxy flow rate

The GPC with different LiOxy flows has also been tested, keeping the NitPhO flow constant at f_3, a process temperature T_3, and over 2000 cycles, as shown in figure 3.3.

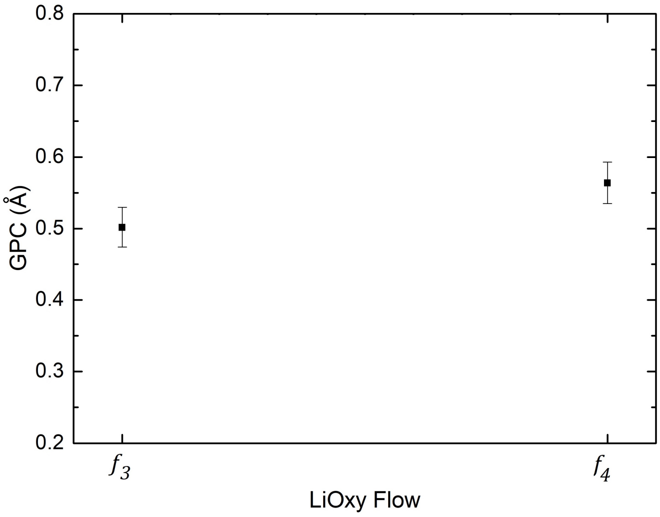

Figure 3.3: GPC according with the LiOxy flow.

Although flow $f_4 = 2f_3$, the GPC is not significantly altered, specially considering that the y-axis is in Å, Therefore, one can conclude that the LiOxy flow has no significant impact on the thin film growth. This might be caused by the saturation of the growth at both precursor in both precursor flow settings.

3.1.4 Precursor exposure time

The exposure time is directly related to the substrate holder rotation speed, usually defined in rotations per minute (RPM). Higher RPM values correspond to shorter exposure times. In this thesis, the rotational speed range is studied from 10 to 60 rpm, which corresponds to an approximate exposure of precursors between 400 ms and 66.7 ms, respectively.

Figure 3.4 shows the impact of process speed on the GPC while keeping the process temperature at T_3, NitPhO and LiOxy flows at f_3 and f_4, respectively.

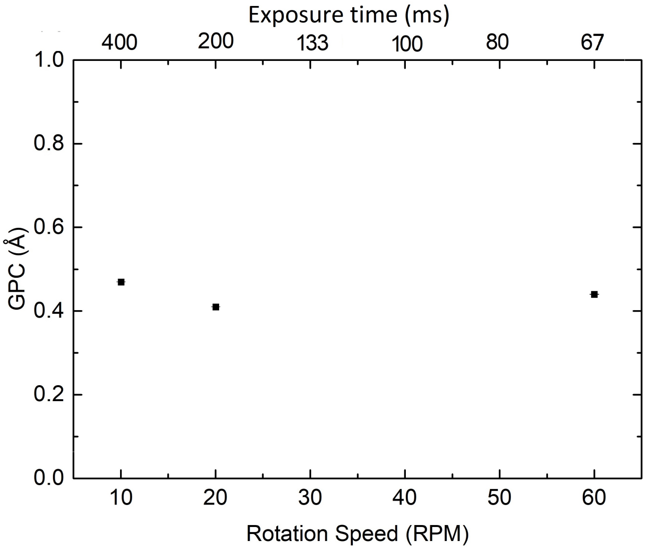

Figure 3.4: GPC according with the rotation speed.

As supposed in a well-behaved *s*ALD deposition, the exposure time does not present a significant effect in the GPC, changing from 0.47 Å/cycle at 10 rpm to 0.44 Å/cycle at 60 rpm, suggesting that the applied exposure time for each of the two precursors is sufficient to reach saturation.

3.2 Film characterization

3.2.1 Thickness profiles

The general thickness profile is determined on sample cross section using SEM measurements. The average thickness of LiPON is calculated from the SEM images taken over the deposition radius. Figure 3.5 represents the thickness profile of a deposited film. It is considered that the position 0 mm corresponds to the inner part of the deposition and 60 mm to the outer part, as represented in the scheme attached.

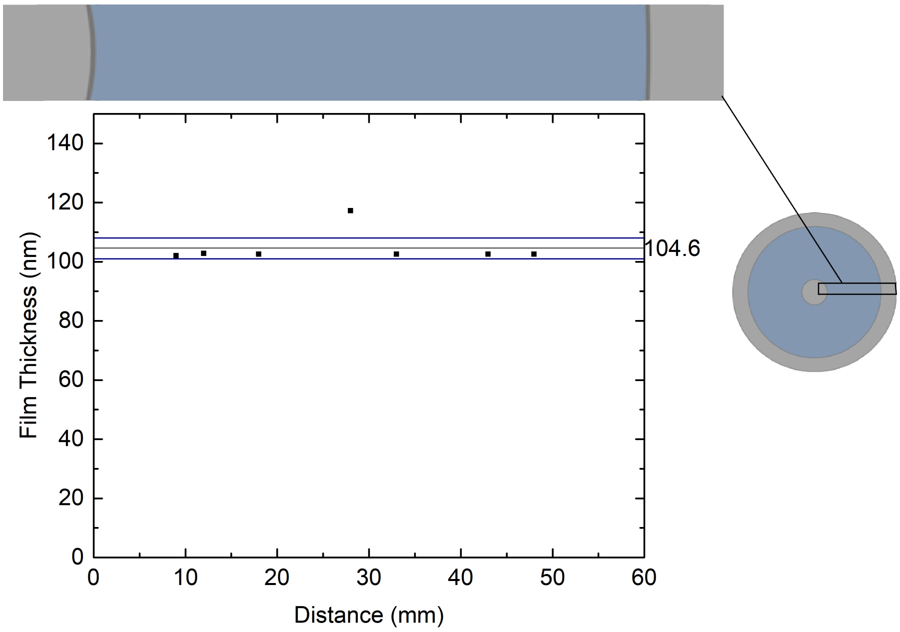

Figure 3.5: Example of film thickness profile as a function of the sample radius.

The optimized process produces a uniform layer across the entire deposition area. No significant differences were found, except on the boundaries of the deposition area which show some differences due to the hardware design of the deposition head and sample holder. Sporadically, some irregularities are found in the films as the measurement found before 30 mm with a thickness around 115 nm. All the posterior analysis are focused in the central part of the deposition.

3.2.1.1 Uniformity

Considering that edge problems can be ignored, (since in an industrial environment the *s*ALD might not be rotational) and in otimized depositions, the sample layer thickness scheme shown in figure 3.5, has an average thickness of 104 ± 2 nm. That corrresponds to 2 % dispersion, which is characteristic of an ideal ALD proces and an optimum property since the targeted dispersion is 5 %. To support the uniformity measurements, figure 3.6 shows two representative SEM images with respective LiPON thickness in different parts of the deposition radius. Note that the 58.6 nm in fig 3.6 a) is relative to the Pt layer under the LiPON.

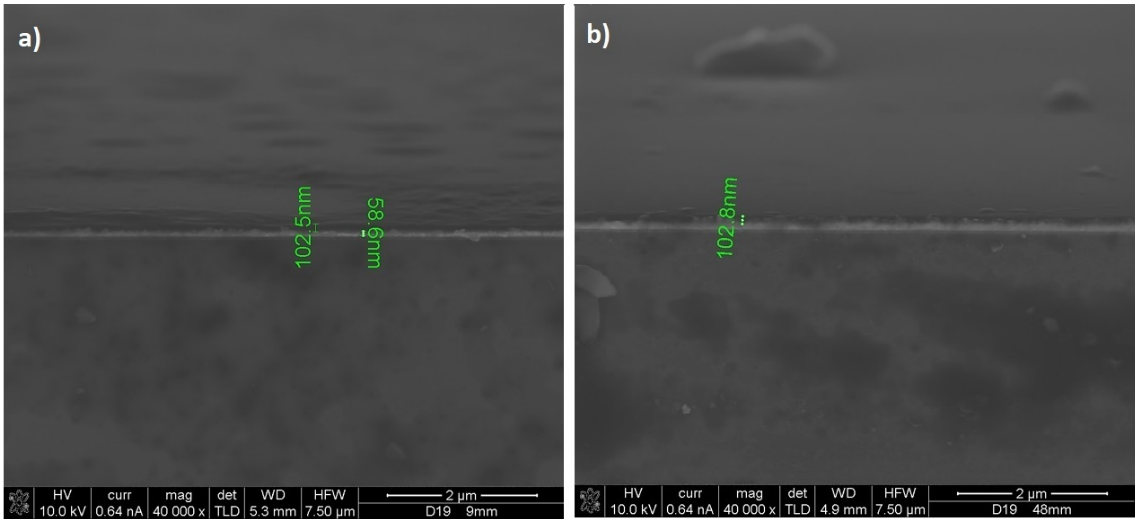

Figure 3.6: Two SEM pictures of the same sample in different deposition radius: a) 9mm; b) 48mm.

However, in non-optimized samples, one feature visible to the eye is the presence of coloured rings. Their colour and intensity changes according the substrate used, the number of cycles or the deposition temperature.

This problem can be analysed further by using profilometry and scanning the sample radius surface even if is air exposed. Figure 3.7 exhibits the profile of the sample produced at T_1, with rings separated exactly 0.5 mm apart and a height difference of 200 nm from the average thickness, 400 nm.

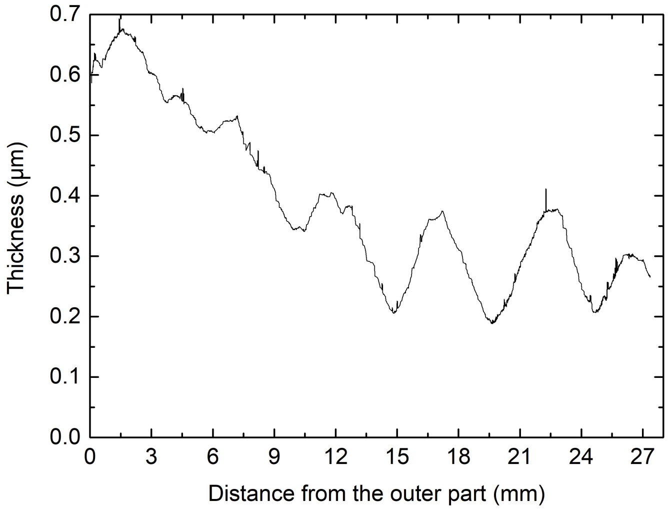

Figure 3.7: Side profile of sample from the outer part until the center of deposition.

This is caused due to the combination of Argon bearings and precursors flow in the reactor head as can be seen in figure 3.8a), the Ar bearings are 5 mm apart. Other interesting fact is that different deposition temperatures affect the amount of rings. With higher process deposition temperatures the number of rings decrease when compared with lower. As stated before, this is due the temperature window of *s*ALD. When the precursor total flow decreases in a certain proportion to the bearing flow, the uniformity improves.

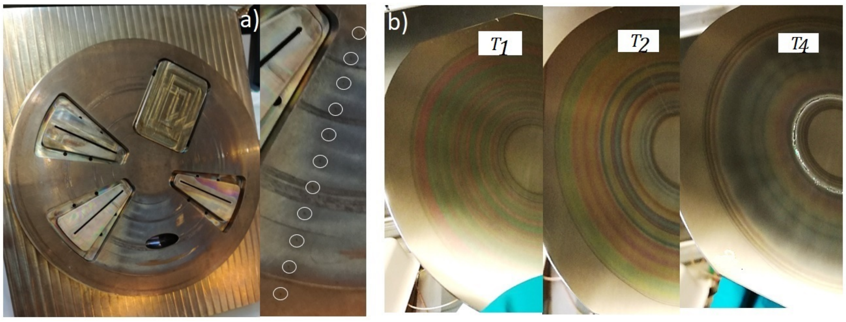

Figure 3.8: a) Reactor head and gas bearing outlets; b) Presence of rings at different temperatures.

3.2.1.2 Film roughness

The film roughness is another interesting growth characteristic. From figure 3.9 we can conclude that the roughness increases directly with the process temperature. We note that this is related with the *s*ALD process temperature.

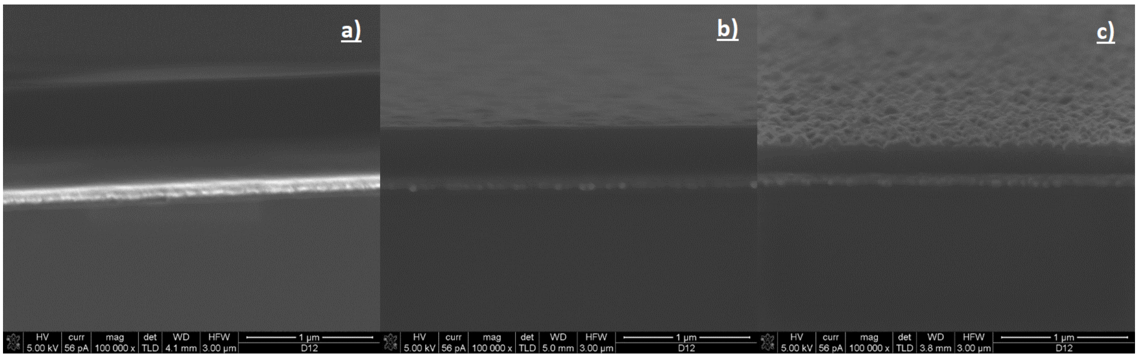

Figure 3.9: SEM images of LiPON films with the same settings and different process temperatures: a)T_1; b)T_2; c)T_4.

3.2.2 Film composition

XPS measurements have been carried out in a Quantera SXM^{TM} from ULVAC using monochromatic AlKα-radiation (25 Watt) with a take-off angle θ of 45°. At this angle the information depth is approximately 7 nm with a spot size of 100 µm scanned across an area of 500 x 500 µm^2. By means of wide scan measurements the elements present at the surface have been identified. Accurate narrow scans were measured for quantification. Standard sensitivity factors were used to convert peak areas to atomic concentrations.

Concentration depth profiles have been determined by alternating measurements and ion bombardment with Ar ions at 2 kV, in a raster of 3.0 x 3.0 mm^2. The sputter rate was calibrated on SiO_2 to be 5 nm/min.

The main goal of this characterization is to determine the LiPON thin film chemical composition which is usually challenging, since such material tends to react with air and other environmental contaminants, forming a compositional gradient in the XPS spectra. In figure 3.10 the upper initial nanometers show a clear discrepancy of the atomic concentrations when compared with bulk composition. For this reason all the following XPS analysis results will be focused on the bulk stoichiometry.

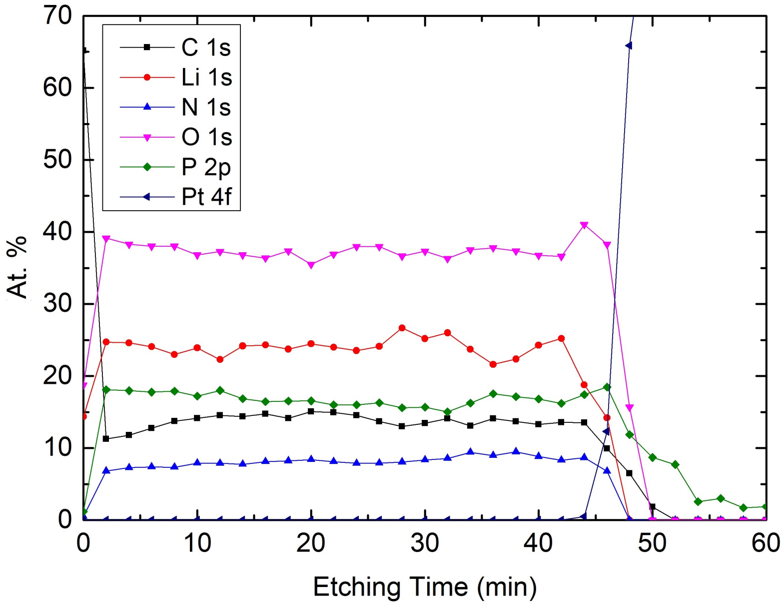

Figure 3.10: XPS depth profile spectra of a representative sample deposited at T_2

The chemical states presented in the deposited LiPON are shown in table 3.1 and figure 3.11 The impact of deposition temperature on the films stoichiometry is investigated.

The LiPON thin films produced at T_2 and T_3 have three phases incorporated:

- Li_2O from the O peak at 528.3 eV and the Li peak at 53.8 eV. Notice that the ratio Li to O is 2:1. Another interesting characteristic is that the Li_2O concentration increases directly with the process temperature and is not detected in the film deposited at T_1. It is well known that Li_2O formation requires high ALD temperature;
- $Li_XPO_YN_Z$, the main chain;
- Carbon contamination as a result of remaining precursor fragments.

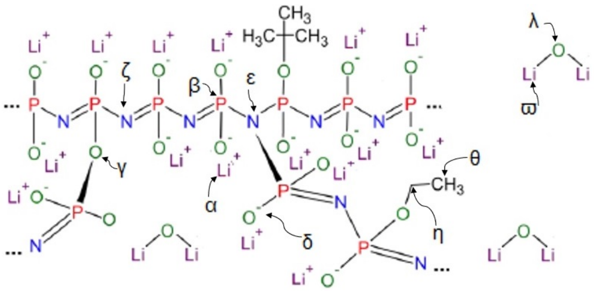

Figure 3.11: A schematic of the proposed molecular structure in the LiPON thin films developed. Adapted from Pearse et al [23].

Table 3.1: XPS quantification of *s*ALD LiPON films synthesized at different process temperatures, T_1, T_2, T_4.

		T_1	T_2	T_4
	B. E.	Atomic Concentration (%)		
α	55.3	24.1	27.7	22.8.1
φ	53.8	0.0	2.2	11.6
β	133.2	13.4	12.1	11.5
γ	532.7	1.9	1.5	2.4
δ	531.0	36.1	35.2	2.4
λ	528.3	0.0	1.2	5.7
ε	299.1	3.5	2.8	1.5
ζ	397.4	4.4	4.1	1.8
η	286.8	2.4	2.5	0.6
θ	284.8	10.4	6.5	1.7

B. E. = Binding Energy

$T_1 < T_2 < T_4$

We calculate the film stoichiometry by normalizing the atomic percentages to phosphorus as well as by excluding the carbon and Li_2O contaminations. The results are presented in table 3.2

Table 3.2: *s*ALD LiPON films final stoichiometry.

Growth Temperature	Atomic Concentration (%)					Comp. relative to P*
	Li	P	O	N	C	
T_1	22.3	18.0	37.3	7.9	14.5	$Li_{1.8}P_{1.0}O_{2.8}N_{0.6}$
T_2	29.8	15.4	38.0	7.1	9.8	$Li_{2.2}P_{1.0}O_{2.9}N_{0.6}$
T_4	32.5	13.4	46.6	3.4	4.0	$Li_{2.0}P_{1.0}O_{3.4}N_{0.3}$

$T_1 < T_2 < T_4$

*Excluding carbon and Li_2O contributions.

Nitrogen and lithium concentrations fall in the range of reported values for ALD deposited LIPON, which is already an indication of ion-conducting LiPON [24, 25].

3.2.3 Reproducibility

In terms of thickness and composition the samples appear to have a good reproducibility. When produced with the same settings even in different days exhibit an acceptable coherence, displaying the same tendency.

3.2.4 Crystal structure

The *s*ALD thin films have been characterized in terms of structure through XRD. This analysis is particularly important since it is reported in literature that amorphous LiPON thin films have higher ionic conductivities than single crystal or polycrystalline films [26] [27].

The obtained XRD data is shown in figure 3.12, excluding the Si and Pt peaks, for samples deposited with different temperatures and is possible to conclude that the three are amorphous. The peaks visible in the figure happen due to the dome in which the samples were being analysed.

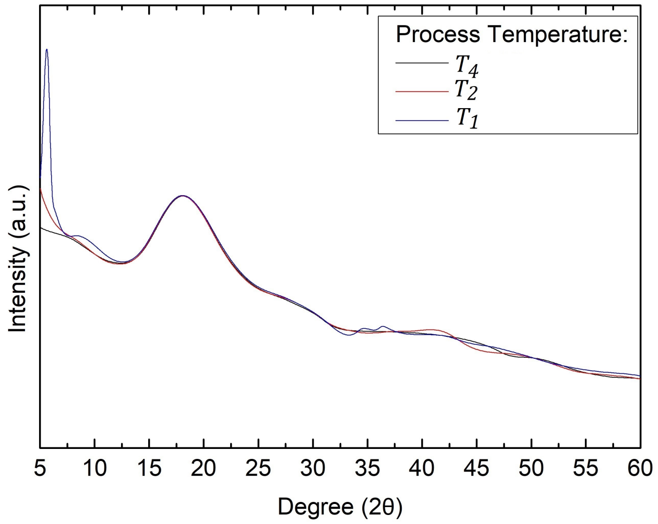

Figure 3.12: XRD patterns of LiPON thin films processed under different temperatures. The remain peaks are atributed to the dome where the samples were inserted.

3.3 Electrochemical Impedance Spectroscopy

To measure the thin film's conductivity the solid state setup was used as described in chapter 2, section 2.7. The first measurements were performed by just placing the two probes in a reference (Pt) sample to check the resistance of the material.

The impedance results as plotted in the complex plane for LiPON include a semicircular arc at high frequencies followed by a rapid increase in the imaginary component of the impedance at low frequencies concurrent with the double-layer formation on the blocking electrodes.

The impedance results are analysed in function of the ALD process temperature. After some initial tests was possible to verify at room temperature, that the sample deposited at temperature T_3, has higher conductivity, 1.55 (± 0.14) x 10^{-7} S/cm when compared with samples performed at T_4, 3.49 (± 0.96) x 10^{-9} S/cm and T_2, 6.83 (± 0.44) x 10^{-10} S/cm.

All further tests have been performed in samples produced at T_3 and T_4. The films synthesized at low temperatures, T_1 and T_2 could not be analysed for their ionic conductivity, probably due to their high out-of-range impedance values.

Figure 3.13 shows LiPON deposited at T_3 impedance results plotted on the complex plane for 4 different measurement temperatures and figure 3.14 LiPON deposited at T_4 impedance results for 6 different measurement temperatures.

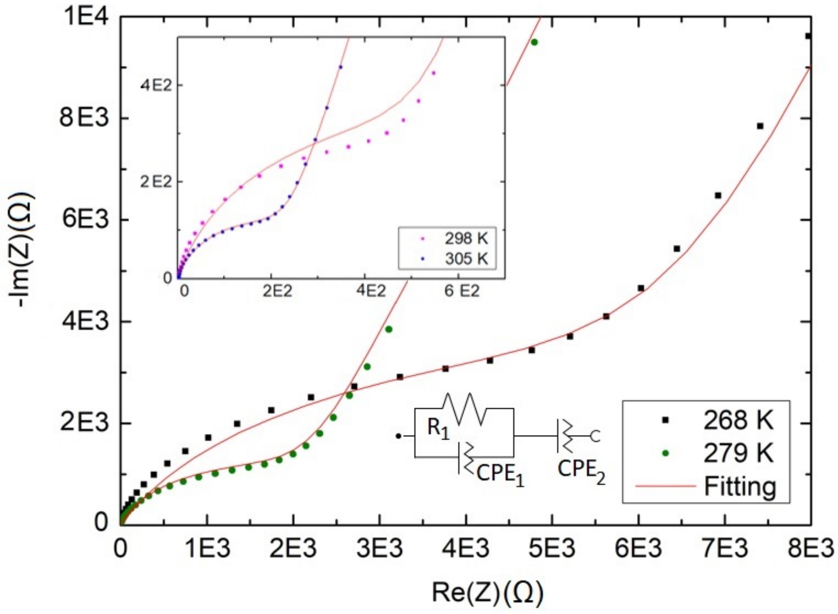

Figure 3.13: Impedance spectra scanned at different measurement temperatures for LiPON films growth at T_3.

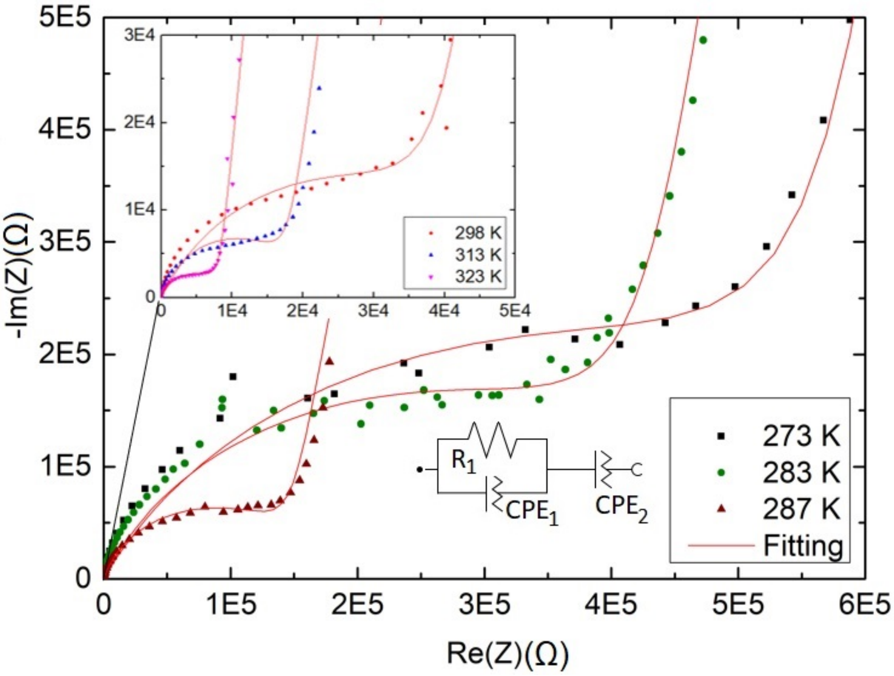

Figure 3.14: Impedance spectra scanned at different measurement temperatures for LiPON films growth at T_4.

By varying the measurement temperature, one may often be able to split the different contributions in the high-frequency region. Yet in our case, this phenomenon was not observed. Therefore, we can conclude that the high-frequency resistance increases with decreasing temperatures.This tend can be ascribed to the fact that ions tend to diffuse slower at lower temperatures.

This plots exhibit the expected components of an impedance measure, this is, the semicircular arc at high frequencies and a straight line at low.

The fit is modelled with a variation of the Randles model. In this case, the equivalent electric circuit shown in figures 3.13 and 3.14. Is constituted by a parallel between the film bulk resistance, R_1 and a constant phase elements (CPE), CPE_1 in series with other CPE that corresponds to the double layer formation on the blocking electrodes.

R_1 and CPE_1 are responsible for the electrolyte's ionic resistance and dielectric capacitance, respectively. In this plots no solid electrolyte interfaces (SEI) are found, meaning that the transition between layers adds no resistance to the final circuit.

As stated, the ionic conductivity of the films is extrapolated from the resistance in the data analysis and calculated through the following expressions (Equations (3.1) and (3.2)).

$$\rho = R\frac{A}{d} \tag{3.1}$$

$$\sigma = \frac{1}{\rho} \tag{3.2}$$

ρ is the film's resistivity, σ the conductivity, A is the circular copper contact area, (diameter is 0.4 cm), and d is the electrolyte thickness, in this case 109 nm for T_3 and 185 nm for T_4. In table 3.3 all the parameters fitted are summarized, with the measurement temperature expressed in kelvin in order to facilitate the derivation of the activation energy.

Table 3.3: Electrical parameters measured in samples characterized at different temperatures.

Deposition temperature	Measurement temperature (K)	Resistance (Ω)	Resistivity ($\Omega.cm$)	Conductivity (S/cm)
T_3	268.2	6.3 x 10^{3}	7.3 x 10^{7}	1.4 x 10^{-8}
	279.2	2.0 x 10^{3}	2.3 x 10^{7}	4.3 x 10^{-8}
	298.2	5.6 x 10^{2}	6.4 x 10^{6}	1.6 x 10^{-7}
	305.7	2.2 x 10^{2}	2.6 x 10^{6}	3.9 x 10^{-7}
T_4	273.2	6.0 x 10^{5}	4.1 x 10^{9}	2.5 x 10^{-10}
	283.0	4.4 x 10^{5}	3.0 x 10^{9}	3.4 x 10^{-10}
	287.0	1.5 x 10^{5}	9.8 x 10^{8}	1.0 x 10^{-9}
	298.0	4.2 x 10^{4}	2.9 x 10^{8}	3.5 x 10^{-9}
	313.0	1.8 x 10^{4}	1.2 x 10^{8}	8.2 x 10^{-9}
	323.0	8.3 x 10^{3}	5.6 x 10^{7}	1.8 x 10^{-8}

Deposition temperature	Measurement temperature (K)	Y_{01} (S)	N_1	Y_{02} (S)	N_2
T_3	268.2	3.5 x 10^{-7}	0.738	1.0 x 10^{-6}	0.841
	279.2	1.7 x 10^{-7}	0.832	1.1 x 10^{-6}	0.820
	298.2	5.0 x 10^{-7}	0.786	1.3 x 10^{-6}	0.878
	305.7	3.2 x 10^{-7}	0.794	2.4 x 10^{-6}	0.813
T_4	273.2	9.8 x 10^{-8}	0.695	7.2 x 10^{-7}	0.950
	283.0	8.3 x 10^{-8}	0.738	7.2 x 10^{-7}	0.932
	287.0	5.8 x 10^{-8}	0.825	7.4 x 10^{-7}	0.905
	298.0	3.0 x 10^{-7}	0.650	1.1 x 10^{-6}	0.934
	313.0	3.4 x 10^{-7}	0.751	1.2 x 10^{-6}	0.905
	323.0	3.4 x 10^{-7}	0.684	1.4 x 10^{-6}	0.927

Y_{01}, N_1, Y_{02} and N_2 are electrical parameters that characterize CPE_1 and CPE_2, respectively. As N changes from 0 to 1 the CPE response evolves from a pure resistor to a capacitor. From the Arrhenius equation (see equation (3.3)), it is possible to derive the activation energy value, converting it in an Arrhenius plot as shown in figure 3.15.

Table 3.4: Electrical parameters measured in for LiPON samples grown at different precursor flows rates.

NitPhO flow	Resistance (Ω)	Resistivity (Ω.cm)	Conductivity (S/cm)
f_1	5.6E x 10^2	6.4 x 10^6	1.6 x 10^{-7}
f_2	2.3E x 10^4	3.5 x 10^8	2.8 x 10^{-9}

$$\sigma = Ae^{\frac{-E_a}{K_B T}} \equiv ln\sigma = lnA - \frac{E_a}{K_B}\frac{1}{T}. \tag{3.3}$$

A is a pre-exponential factor, E_a is the activation energy, K_B the Boltzman constant and T the measurement temperature.

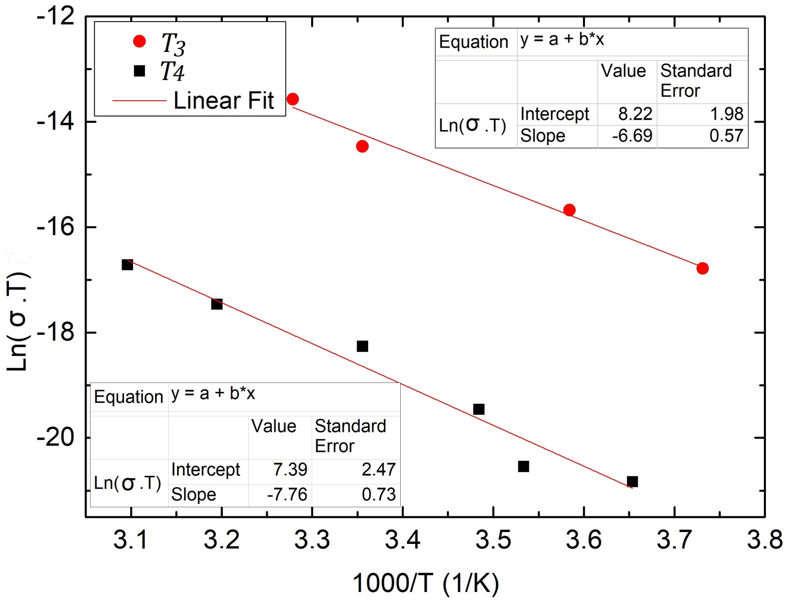

Figure 3.15: Arrhenius plot fot Li-conduction through LiPON electrolyte samples synthetized at T_3 and T_4.

The activation energy for Li-conduction through the electrolyte synthesized at T_3 and T_4 is 0.58 (± 0.01) eV and 0.69 (± 0.01) eV, respectively. Both values are high when compared with previous studies in this area (0.55 ± 0.01 eV) [23].

The influence of NitPhO flows has also been analysed in terms of ionic conductivity keeping the LiOxy flow at f_4. In figure 3.16 the complex plots for samples measured at room temperature are represented and in table 3.4 the respective ionic resistances and conductivities can be seen.

Despite the fact that the NitPhO does not affect the GPC, it appears that increasing the flow, the electrolyte ionic conductivity decreases.

The electronic conductivity was also measured to check if the electrolyte sufficiently prevents any electron conduction through it. Here a 2V constant potential

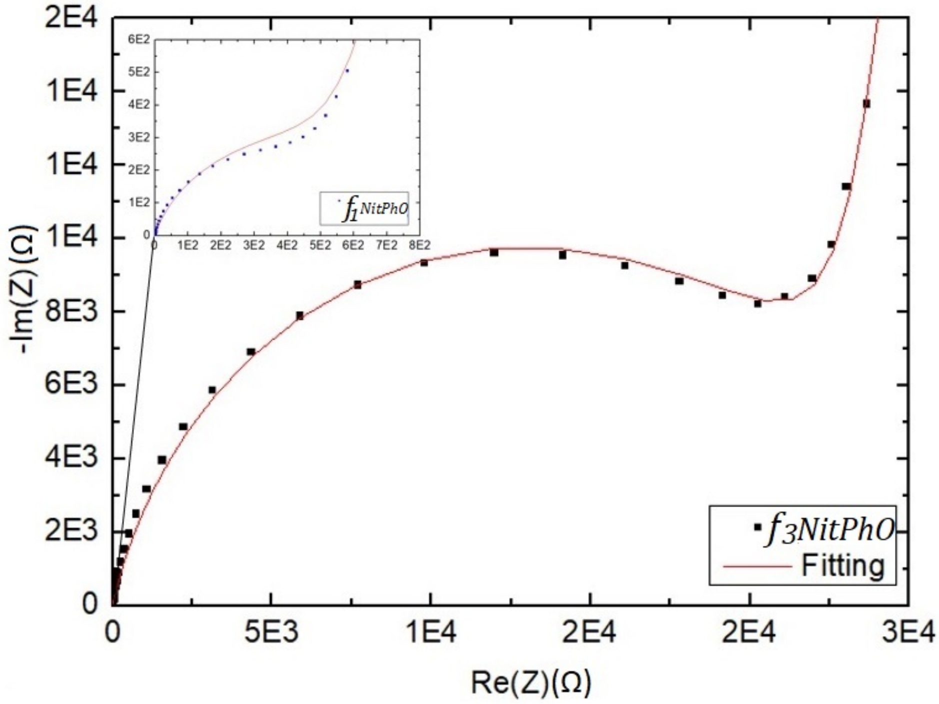

Figure 3.16: Complex impedance plots of LiPON samples grown with different NitPhO precursor flows.

Table 3.5: Overview of electronic, ionic conductivity and process time of LiPON thin film produced in this thesis and in articles with similar methods and precursors.

	This work	Ref. [23]	Ref. [20]	
σ_{ionic} (S/cm)	2.38 x 10^{-7}	6.51 x 10^{-7}	9.3 x 10^{-8}	6.6 x 10^{-7}
$\sigma_{electronic}$ (S/cm)	1.86 x 10^{-13}	4.4 x 10^{-13}	3.3 x 10^{-12}	3.3 x 10^{12}
Process time (s/nm)	18.35	696.5	240	240

is applied over the Pt/LiPON/Cu stack while measuring the current through the electrolyte over time, see figure 3.17. It's clear that the current decreases rapidly to extremely low values. After 200 sec. a relatively stable leakage current of 4.3 x 10^{-9} A is measured and the corresponding electronic conductivity is 1.86 x 10^{-13} S/cm. This is in the targeted order for this thesis work.

Comparing the results obtained with literature is possible to see that the values are extremely good taking into account the process time, see table 3.5.

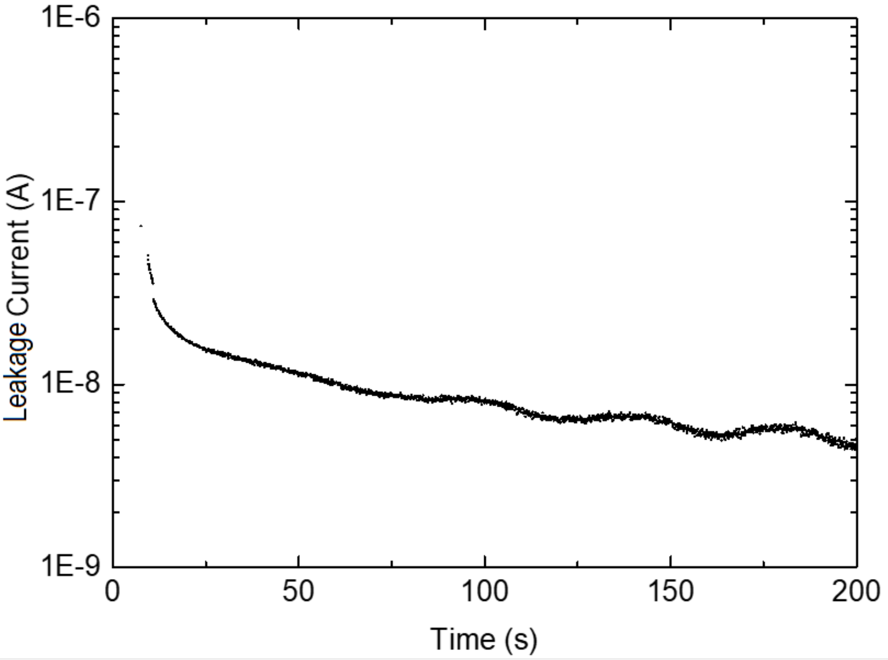

Figure 3.17: Current-time response from a 2V constant potential applied across a typical Pt/LiPON/Cu stack.

4 Conclusions and future perspectives

The synthesis of LiPON through *s*ALD is successful when using the LiOxy and NitPhO precursors. The impacts of the process parameters on the deposited films are addressed. At T_1 the film growth does not follow an ALD regime and its conductivity could not be measured. Furthermore, the thin film has a relatively high atomic concentration of carbon and oxygen.

Oppositely, the sample grown at T_3 exhibits the best ionic conductivity 2.38 (± 0.14) x 10^{-7} S/cm and electronic 1.86 x 10^{-13} S/cm.

The presence of Li_2O as well as the low nitrogen content decrease the ionic conductivity of the films deposited atT_2 and T_4.

The precursors flow has impact on the GPC and conductivity as well, lower NitPhO and higher LiOxy flows improve the conductivity. The rotation speed variation doesn't affect the GPC.

The variation of temperature in electrochemical measurements reflects in the complex plot real part, directly relating increased conductivities in higher temperature measurements since the resistance decreases. The opposite behaviour might be observed as well. The plots were fitted with an equivalent electric circuit containing a parallel of a resistance, R_1 with a constant phase elements, CPE $_1$, both in series with another constant phase element, CPE $_2$. The fittings were successful and a value for each electronic element was found, from R_1 and the electronic conductivity for each film is measured.

The best activation energy obtained corresponds to 0.58 ± 0.01 eV, which is a value comparable to literature.

In TNO and in other battery research groups the studies are now dedicated to apply LiPON films in 3D structures, thus improving the conductivity, including studies on film annealing under vacuum or in purified nitrogen atmosphere. There is also the possibility to use other precursors and test other electrolytes compositions.

Bibliography

[1] J.-K Park. "Principles and Applications of Lithium Secondary Batteries." In: (Aug. 2012).

[2] P. Sehrawat, C. Julien, and S. Islam. "Carbon nanotubes in Li-ion batteries: A review." In: *Materials Science and Engineering: B* 213 (2016), pp. 12 –40.

[3] A. Sieminski. *Annual Energy Outlook 2016*. Energy Information Administration, 2016.

[4] R. Huggins. *Advanced batteries: materials science aspects*. Springer Science & Business Media, 2008.

[5] M. Mancini, E. Bekaert, T. Diemant, M. Marinaro, L. de Biasi, R. Behm, and M. Wohlfahrt-Mehrens. "Study on the stability of Li2MnSiO4 cathode material in different electrolyte systems for Li-ion batteries." In: *Electrochimica Acta* 176 (2015), pp. 679 –688.

[6] M. Mäntymäki. "Atomic Layer Deposition and Lithium-ion Batteries : Studies on new materials and reactions for battery development." In: 2017.

[7] X. Xie, S. Wang, K. Kretschmer, and G. Wang. "Two-dimensional layered compound based anode materials for lithium-ion batteries and sodium-ion batteries." In: *Journal of colloid and interface science* 499 (2017), pp. 17–32.

[8] J. Kalhoff, G. G. Eshetu, D. Bresser, and S. Passerini. "Safer Electrolytes for Lithium-Ion Batteries: State of the Art and Perspectives." In: *ChemSusChem* 8.13 (), pp. 2154–2175.

[9] M. Roberts, P. Johns, J. Owen, D. Brandell, K. Edstrom, G. El Enany, C. Guery, D. Golodnitsky, M. Lacey, C. Lecoeur, et al. "3D lithium ion batteries—from fundamentals to fabrication." In: *Journal of Materials Chemistry* 21.27 (2011), pp. 9876–9890.

[10] Y. Zargouni, S. Deheryan, A. Radisic, K. Alouani, and P. M. Vereecken. "Electrolytic manganese dioxide coatings on high aspect ratio micro-pillar arrays for 3D thin film lithium ion batteries." In: *Nanomaterials* 7.6 (2017), p. 126.

[11] A. Pearse, T. Schmitt, E. Sahadeo, D. M. Stewart, A. Kozen, K. Gerasopoulos, A. A. Talin, S. B. Lee, G. W. Rubloff, and K. E. Gregorczyk. "Three-Dimensional Solid-State Lithium-Ion Batteries Fabricated by Conformal Vapor-Phase Chemistry." In: *ACS nano* 12.5 (2018), pp. 4286–4294.

[12] C. Frijters, P Poodt, and A Illiberi. "Atmospheric spatial atomic layer deposition of Zn (O, S) buffer layer for Cu (In, Ga) Se2 solar cells." In: *Solar Energy Materials and Solar Cells* 155 (2016), pp. 356–361.

[13] A Illiberi, R Scherpenborg, Y Wu, F Roozeboom, and P Poodt. “Spatial Atmospheric Atomic Layer Deposition of Al x Zn1−x O.” In: *ACS applied materials & interfaces* 5.24 (2013), pp. 13124–13128.

[14] Y. Cao, X. Meng, and J. W. Elam. “Atomic Layer Deposition of LixAlyS Solid-State Electrolytes for Stabilizing Lithium-Metal Anodes.” In: *ChemElectroChem* 3.6 (2016), pp. 858–863.

[15] M. Létiche, E. Eustache, J. Freixas, A. Demortière, V. De Andrade, L. Morgenroth, P. Tilmant, F. Vaurette, D. Troadec, P. Roussel, et al. “Atomic Layer Deposition of Functional Layers for on Chip 3D Li-Ion All Solid State Microbattery.” In: *Advanced Energy Materials* 7.2 (2017), p. 1601402.

[16] B. Wang, J. Liu, Q. Sun, R. Li, T.-K. Sham, and X. Sun. “Atomic layer deposition of lithium phosphates as solid-state electrolytes for all-solid-state microbatteries.” In: *Nanotechnology* 25.50 (2014), p. 504007.

[17] Y. Zhu, X. He, and Y. Mo. “Origin of outstanding stability in the lithium solid electrolyte materials: Insights from thermodynamic analyses based on first-principles calculations.” In: *ACS applied materials & interfaces* 7.42 (2015), pp. 23685–23693.

[18] Y. Hamon, A Douard, F Sabary, C Marcel, P. Vinatier, B. Pecquenard, and A. Levasseur. “Influence of sputtering conditions on ionic conductivity of LiPON thin films.” In: *Solid State Ionics* 177.3-4 (2006), pp. 257–261.

[19] A. C. Kozen, A. J. Pearse, C.-F. Lin, M. Noked, and G. W. Rubloff. “Atomic layer deposition of the solid electrolyte LiPON.” In: *Chemistry of Materials* 27.15 (2015), pp. 5324–5331.

[20] M. Nisula, Y. Shindo, H. Koga, and M. Karppinen. “Atomic layer Deposition of lithium phosphorus oxynitride.” In: *Chemistry of Materials* 27.20 (2015), pp. 6987–6993.

[21] C. Choi, W. Cho, B. Cho, H. Kim, Y. Yoon, and Y. Tak. “Radio-frequency magnetron sputtering power effect on the ionic conductivities of LiPON films.” In: *Electrochemical and solid-state letters* 5.1 (2002), A14–A17.

[22] B. Put, M. J. Mees, N. Hornsveld, P. M. Vereecken, W. Kessels, and M. Creatore. “Plasma-assisted ALD of LiPO (N) for solid state batteries.” In: *Meeting Abstracts*. 3. The Electrochemical Society. 2016, pp. 347–347.

[23] A. J. Pearse, T. E. Schmitt, E. J. Fuller, F. El-Gabaly, C.-F. Lin, K. Gerasopoulos, A. C. Kozen, A. A. Talin, G. Rubloff, and K. E. Gregorczyk. “Nanoscale solid state batteries enabled by thermal atomic layer deposition of a lithium polyphosphazene solid state electrolyte.” In: *Chemistry of Materials* 29.8 (2017), pp. 3740–3753.

[24] K. Senevirathne, C. S.Day, M. D. Gross, and A. L. abd N.A.W. Holzwarth. “A new crystalline LiPON electrolyte: Synthesis, properties, and electronic structure.” In: *Solid State Ionics* 233.1 (2013), pp. 95–101.

[25] É. Guille, G. Vallverdu, and I. Baraille. "First Principle calculation of core level binding energies of LixPOyNz solid electrolyte." In: *The journal of chemical physics* 141.24 (2014), p. 244703.

[26] Y. G. Kim. *Plasma-assisted directed vapor deposition for synthesizing lithium phosphorus oxynitride thin films*. 2008.

[27] Y. G. Kim and H. Wadley. "Lithium phosphorous oxynitride films synthesized by a plasma-assisted directed vapor deposition approach." In: *Journal of Vacuum Science & Technology A: Vacuum, Surfaces, and Films* 26.1 (2008), pp. 174–183.